

ARPIST: Provably Accurate and Stable Numerical Integration over Spherical Triangles

Yipeng Li^{a,b}, Xiangmin Jiao^{a,*}

^a*Dept. of Applied Math. & Stat. and Institute for Advanced Computational Science, Stony Brook University, Stony Brook, NY 11794, USA.*

^b*Current address: Beijing Oneflow Technology Ltd., Haidian District, Beijing, 100083, China*

Abstract

Numerical integration on spheres, including the computation of the areas of spherical triangles, is a core computation in geomathematics. The commonly used techniques sometimes suffer from instabilities and significant loss of accuracy. We describe a new algorithm, called *ARPIST*, for accurate and stable integration of functions on spherical triangles. *ARPIST* is based on an easy-to-implement transformation to the spherical triangle from its corresponding linear triangle via radial projection to achieve high accuracy and efficiency. More importantly, *ARPIST* overcomes potential instabilities in computing the Jacobian of the transformation, even for poorly shaped triangles that may occur at poles in regular longitude-latitude meshes, by avoiding potential catastrophic rounding errors. We compare our proposed technique with L'Huilier's Theorem for computing the area of spherical triangles, and also compare it with the recently developed LSQST method (J. Beckmann, H.N. Mhaskar, and J. Prestin, *GEM - Int. J. Geomath.*, 5:143–162, 2014) and a radial-basis-function-based technique (J. A. Reeger and B. Fornberg, *Stud. Appl. Math.*, 137:174–188, 2015) for integration of smooth functions on spherical triangulations. Our results show that *ARPIST* enables superior accuracy and stability over previous methods while being orders of magnitude faster and significantly easier to implement.

Keywords: Surface integration, accuracy and stability, spherical triangles

*Corresponding author

Email addresses: jamesonli1313@gmail.com (Yipeng Li),
xiangmin.jiao@stonybrook.edu (Xiangmin Jiao)

1. Introduction

Applications in geophysics often require solving partial differential equations (PDEs) on spherical geometries using numerical methods, such as finite element and finite volume methods. A critical component is the computation of numerical integration over the elements or cells of a surface mesh discretizing a sphere, for example, to compute surface fluxes between the atmosphere and ocean models. Sometimes, it is desirable to compute the integration accurately to near machine precision, for example, when transferring flux quantities under the constraint of global conservation. In these applications, one often needs to integrate over a spherical n -gon. In this work, we focus on integrating functions over spherical triangles, of which the edges are geodesics between the vertices since a spherical n -gon can be tessellated into $n - 2$ triangles.

Despite its importance, accurate and stable computation on spherical triangles has not been resolved satisfactorily in the literature. Classical numerical quadrature (a.k.a. cubature) techniques on spheres have focused on integrating smooth functions over a whole sphere, for example, by determining a minimal number of quadrature points to maximize the exact integration of a maximal number of spherical harmonics or polynomials; see, e.g., the classical papers [1, 2], recent monographs [3, 4], the comprehensive survey article [5] and the references therein, as well as more recent works [6, 7]. Some of these techniques compute the integration using a tessellation of the sphere, such as a spherical Delaunay triangulation [6] or a cubed-sphere mesh [7]. One of the earliest works that focused on integration over spherical triangles is [8], which integrated over a spherical triangle by recursively subdividing it and then using low-degree quadrature rules. Such a technique, however, may require too many splittings to reach (near) machine precision. Beckmann et al. [9] proposed the so-called LSQST, which uses QR factorization to compute quadrature weights on each spherical triangle, resulting in superlinear complexity in the number of quadrature points. In addition, LSQST suffers from numerical instabilities [9, Remark 2.3]. Recently, A. Sommariva et al. [10, 11] used perpendicular projection and quadrature rules on elliptical sectors for spherical

integration, which can reach machine precision with a high degree quadrature rule (e.g., $n = 20$) on a sphere octant. Another recent work, SphericalQuadratureRBF (or SQRBF in short) [12, 6], utilizes radial-basis functions in computing integration on a spherical triangulation.

In this work, we propose a new technique called *anchored radially projected integration on spherical triangles* or *ARPIST*. The core idea of ARPIST is to utilize the transformation to the spherical triangle from its corresponding linear triangle via a radial projection. Although this idea is simple, care must be taken to ensure the stable computation of the Jacobian determinant of the transformation. We prove that ARPIST can overcome potential instabilities, even for poorly shaped triangles, such as those near poles in a regular latitude-longitude (RLL) mesh or the triangles in overlay meshes in remapping algorithms [13]. We overcome the instabilities by properly selecting one of the vertices as the “anchor” when computing the Jacobian determinant to avoid catastrophic cancellation errors. As a result, ARPIST achieves superior accuracy and stability, reaching (near) machine precision with an adaptive-refinement procedure. ARPIST is also highly efficient: It requires only linear time complexity in the number of quadrature points per triangle, which is significantly more efficient than LSQST. In addition, ARPIST is much easier to implement than LSQST [9] and SQRBF [6]. The MATLAB and Python implementations of ARPIST are available at <https://github.com/numgeom/arpist>.

The remainder of the paper is organized as follows. In Section 2, we derive a new algorithm for numerical integration on spherical triangles and analyze its accuracy and stability. In Section 3, we present some comparisons of ARPIST with other techniques in the literature for the computation of the areas of spherical triangles and the integration of smooth functions. Section 4 concludes the paper with some discussions.

2. Accurate and Stable Integration on Spheres

We describe a new algorithm to compute the numerical integration of a sufficiently smooth function over a spherical triangle.

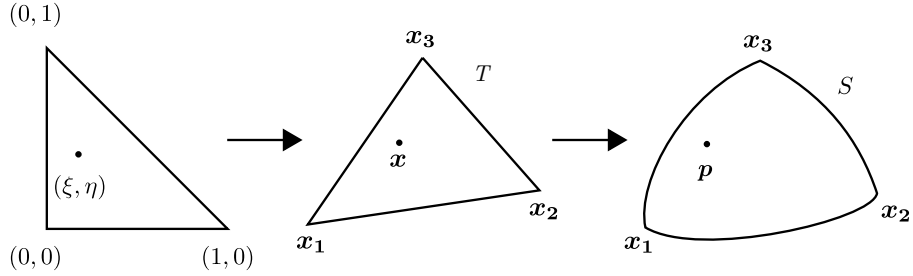


Figure 1: Projection from a reference triangle to a spherical triangle via a linear triangle.

2.1. Integration via radial projection

Consider a spherical triangle S with vertices \mathbf{x}_1 , \mathbf{x}_2 , and \mathbf{x}_3 . Without loss of generality, assume the vertices are in counterclockwise order with respect to the outward normal to the sphere. Let r denote the radius of the sphere, i.e., $r = \|\mathbf{x}_i\|$. Let T denote its corresponding flat (linear) triangle $\mathbf{x}_1\mathbf{x}_2\mathbf{x}_3$, and let (ξ, η) denote the natural coordinates of T , so that T has the parameterization

$$\mathbf{x}(\xi, \eta) = (1 - \xi - \eta)\mathbf{x}_1 + \xi\mathbf{x}_2 + \eta\mathbf{x}_3 \quad (1)$$

for $0 \leq \xi \leq 1$ and $0 \leq \eta \leq 1 - \xi$. Let $\hat{\mathbf{p}}(\mathbf{x}) = r\mathbf{x} / \|\mathbf{x}\|$, which projects a point $\mathbf{x} \in T$ onto a point in S . We then obtain a radial projection

$$\mathbf{p}(\xi, \eta) = \hat{\mathbf{p}}(\mathbf{x}(\xi, \eta)) = r\mathbf{x}(\xi, \eta) / \|\mathbf{x}(\xi, \eta)\|. \quad (2)$$

See Figure 1 for a schematic of the mapping.

Given a function f on the spherical triangle S , the integral is

$$\int_S f(\mathbf{p})dA = \int_0^1 \int_0^{1-\xi} f(\mathbf{p}(\xi, \eta))J d\eta d\xi, \quad (3)$$

where $J = \|\mathbf{p}_\xi \times \mathbf{p}_\eta\|$ is the Jacobian determinant of the mapping from the reference triangle to the curved triangle. The partial derivatives \mathbf{p}_ξ and \mathbf{p}_η have the closed forms

$$\mathbf{p}_\xi = \frac{r}{\|\mathbf{x}\|} \left(\mathbf{x}_2 - \frac{\mathbf{x} \cdot \mathbf{x}_2}{\mathbf{x} \cdot \mathbf{x}} \mathbf{x} \right), \quad (4)$$

$$\mathbf{p}_\eta = \frac{r}{\|\mathbf{x}\|} \left(\mathbf{x}_3 - \frac{\mathbf{x} \cdot \mathbf{x}_3}{\mathbf{x} \cdot \mathbf{x}} \mathbf{x} \right). \quad (5)$$

Note that J varies from point to point, so the computation based on (4) and (5) directly are inefficient to compute. More importantly, the cross product may suffer from instabilities due to cancellation errors when \mathbf{p}_ξ and \mathbf{p}_η are nearly parallel.

To achieve stability and efficiency, we derive a new formula as follows. For brevity, let us use the notation

$$\det[\mathbf{a}, \mathbf{b}, \mathbf{c}] = \begin{vmatrix} a_1 & b_1 & c_1 \\ a_2 & b_2 & c_2 \\ a_3 & b_3 & c_3 \end{vmatrix} = \begin{vmatrix} a_1 & a_2 & a_3 \\ b_1 & b_2 & b_3 \\ c_1 & c_2 & c_3 \end{vmatrix},$$

which is equivalent to the triple product $\mathbf{a} \cdot (\mathbf{b} \times \mathbf{c})$. The following property will turn out to be useful:

$$\det[\mathbf{a}, \mathbf{b}, \mathbf{c}] = \det[\mathbf{a}, \mathbf{b} + s\mathbf{a}, \mathbf{c} + t\mathbf{a}] \quad \forall s, t \in \mathbb{R}. \quad (6)$$

Lemma 1. *Given a spherical triangle S on a sphere with radius r , let \mathbf{x}_1 , \mathbf{x}_2 , and \mathbf{x}_3 be its vertices in counterclockwise order w.r.t. the outward normal to S . Let T be the corresponding linear triangle $\mathbf{x}_1\mathbf{x}_2\mathbf{x}_3$ composed of points $\mathbf{x}(\xi, \eta)$ as in (1). The integral of a continuous function f over S is*

$$\int_S f(\mathbf{p}) dA = r^2 \det[\mathbf{x}_1, \mathbf{x}_2, \mathbf{x}_3] \int_0^1 \int_0^{1-\xi} \frac{f(\mathbf{p}(\xi, \eta))}{\|\mathbf{x}(\xi, \eta)\|^3} d\eta d\xi, \quad (7)$$

where $\mathbf{p}(\xi, \eta)$ is defined in (2).

Proof. Consider \mathbf{p}_ξ and \mathbf{p}_η in (4) and (5). Note that \mathbf{p}_ξ and \mathbf{p}_η are tangent to S , so $\mathbf{p}_\xi \times \mathbf{p}_\eta$ is normal to S and hence is parallel to $\mathbf{x}/\|\mathbf{x}\|$. The area measure J in (3) is then

$$J = \|\mathbf{p}_\xi \times \mathbf{p}_\eta\| = \det\left[\frac{\mathbf{x}}{\|\mathbf{x}\|}, \mathbf{p}_\xi, \mathbf{p}_\eta\right] \quad (8)$$

$$= \frac{r^2}{\|\mathbf{x}\|^3} \det\left[\mathbf{x}, \mathbf{x}_\xi - \frac{\mathbf{x} \cdot \mathbf{x}_\xi}{\mathbf{x} \cdot \mathbf{x}} \mathbf{x}, \mathbf{x}_\eta - \frac{\mathbf{x} \cdot \mathbf{x}_\eta}{\mathbf{x} \cdot \mathbf{x}} \mathbf{x}\right], \quad (9)$$

$$= \frac{r^2}{\|\mathbf{x}\|^3} \det[\mathbf{x}, \mathbf{x}_\xi, \mathbf{x}_\eta], \quad (10)$$

where the last equality is due to (6). From (1), we have

$$\mathbf{x}_\xi = \mathbf{x}_2 - \mathbf{x}_1 \quad \text{and} \quad \mathbf{x}_\eta = \mathbf{x}_3 - \mathbf{x}_1. \quad (11)$$

Substituting (11) and (1) into (10) and using (6), we have

$$J = \frac{r^2}{\|\mathbf{x}\|^3} \det[\mathbf{x}, \mathbf{x}_2 - \mathbf{x}_1, \mathbf{x}_3 - \mathbf{x}_1] \quad (12)$$

$$= \frac{r^2}{\|\mathbf{x}\|^3} \det[\mathbf{x}_1 + \xi(\mathbf{x}_2 - \mathbf{x}_1) + \eta(\mathbf{x}_3 - \mathbf{x}_1), \mathbf{x}_2 - \mathbf{x}_1, \mathbf{x}_3 - \mathbf{x}_1] \quad (13)$$

$$= \frac{r^2}{\|\mathbf{x}\|^3} \det[\mathbf{x}_1, \mathbf{x}_2 - \mathbf{x}_1, \mathbf{x}_3 - \mathbf{x}_1] \quad (14)$$

$$= \frac{r^2}{\|\mathbf{x}\|^3} \det[\mathbf{x}_1, \mathbf{x}_2, \mathbf{x}_3]. \quad (15)$$

Substituting (15) into (3), we then obtain (7). \square

Note that in (8), the triple product $\det[\mathbf{x}/\|\mathbf{x}\|, \mathbf{p}_\xi, \mathbf{p}_\eta]$ is guaranteed to be positive due to the counterclockwise convention of $\mathbf{x}_1\mathbf{x}_2\mathbf{x}_3$, since both \mathbf{x} and $\mathbf{p}_\xi \times \mathbf{p}_\eta$ points outward to S .

Remark 2. Eq. (7) has some vague similarities as (2) in [6], but there are two fundamental differences. First, Reeger and Fornberg used the gnomonic projection [14] to project spherical triangles onto a local tangent plane after rotating the spherical triangle to the top. In contrast, our approach projects the spherical triangles onto the linear triangle radially without requiring any rotation. Second, Reeger and Fornberg expressed the integration in the global xyz coordinate system and then approximated it using radial-basis functions. In contrast, our approach expresses the integration using a local parameterization over the triangle and then integrates the function using standard Gaussian quadrature rules over the linear triangles.

2.2. Radially projected Gaussian quadrature

Utilizing Lemma 1, we then obtain an efficient quadrature rule based on the Gaussian quadrature over the linear triangle T .

Theorem 3. *Given a spherical triangle S on a sphere with radius r and vertices and its corresponding linear triangle T as in Lemma 1, let $\{(\boldsymbol{\xi}_i, w_i) \mid 1 \leq i \leq q\}$ define a degree- p quadrature over T , where the $\boldsymbol{\xi}_i$ are the quadrature points and the w_i are the corresponding weights. If the integrand $f(\mathbf{p}) : S \rightarrow \mathbb{R}$ is continuously differentiable*

to p th order, then

$$\int_S f(\mathbf{p}(\boldsymbol{\xi}))dA = r^2 \det[\mathbf{x}_1, \mathbf{x}_2, \mathbf{x}_3] \sum_i \frac{w_i}{\|\mathbf{x}(\boldsymbol{\xi}_i)\|^3} f(\mathbf{p}(\boldsymbol{\xi}_i)) + A\mathcal{O}(h^{p+1}), \quad (16)$$

where h denotes the longest edge of the triangle and $A = \text{area}(T)$.

This theorem follows from the two-dimensional Taylor series expansion [15] and the high-order chain rule [16], analogous to the proof of one-dimensional quadrature rules. We sketch the argument as follows.

Proof. Let $g(\boldsymbol{\xi})$ denote $f(\mathbf{p}(\boldsymbol{\xi}))/\|\mathbf{x}(\boldsymbol{\xi})\|^3$. Consider the d -dimensional Taylor series expansion of $g(\boldsymbol{\xi})$ with respect to $\boldsymbol{\xi}$ about $\boldsymbol{\xi}_0$ (for example, $\boldsymbol{\xi}_0 = \mathbf{0}$),

$$g(\boldsymbol{\xi}_0 + \mathbf{h}) = \sum_{k=0}^p \frac{1}{k!} \nabla^k g(\boldsymbol{\xi}_0) : \mathbf{h}^k + \frac{C_1 \|\nabla^{p+1} g(\boldsymbol{\xi}_0 + \boldsymbol{\epsilon})\|}{(p+1)!} \|\mathbf{h}\|^{p+1}, \quad (17)$$

where \mathbf{h}^k denotes the k th tensor power of \mathbf{h} , ∇^k denotes the derivative tensor of order k with respect to $\boldsymbol{\xi}$, “:” denotes the scalar product of k th-order tensors, $\|\boldsymbol{\epsilon}\| \leq \|\mathbf{h}\|$, and $|C_1| \leq 1$. A degree- p quadrature rule over the triangle T integrates the first term in (17) exactly. Since $\mathbf{x}(\boldsymbol{\xi})$ and $\mathbf{p}(\boldsymbol{\xi})$ are both smooth and $\|\mathbf{x}(\boldsymbol{\xi})\| = r + \mathcal{O}(h^2) \geq C_2 > 0$, by repeatedly applying the high-order chain rule, we conclude that $\|\nabla^{p+1} g(\boldsymbol{\xi}_0 + \boldsymbol{\epsilon})\|$ is bounded if $f(\mathbf{p})$ is continuously differentiable. Hence, the remainder term in (17) is $\mathcal{O}(h^{p+1})$, and the integral error over T is bounded by $\text{area}(T)\mathcal{O}(h^{p+1})$. \square

Theorem 3 allows us to reuse Gaussian quadrature rules on linear triangles, such as those in [17], to integrate over spherical triangles directly. It is well known that Gaussian quadrature rules can achieve the highest accuracy for a given number of quadrature points over individual triangles, because they are constructed by solving for the quadrature points and the weights to maximize the degree of polynomials that can be integrated exactly (see e.g., [18, Chapter 8]). In (16), $\text{area}(T) = \mathcal{O}(h^2)$ for a triangle T with maximum edge length h . When applying the radially projected quadrature rule on a triangulation of a fixed area on a sphere, the resulting composite quadrature rule is then $(p+1)$ st order accurate if the integrand is continuously differentiable to p th order.

2.3. Stable computation of the determinant

When evaluating (16), a subtle numerical issue is the computation of $\det[\mathbf{x}_1, \mathbf{x}_2, \mathbf{x}_3]$. There are various ways in computing the determinant, and they may have drastically different stability properties when using floating-point arithmetic for small spherical triangles. For example, one could compute the determinants using the triple-product formula

$$\mathbf{a} \cdot (\mathbf{b} \times \mathbf{c}) = a_1(b_2c_3 - b_3c_2) + a_2(b_3c_1 - b_1c_3) + a_3(b_1c_2 - b_2c_1), \quad (18)$$

by substituting $\mathbf{x}_1, \mathbf{x}_2$, and \mathbf{x}_3 as \mathbf{a}, \mathbf{b} , and \mathbf{c} , respectively. This approach, however, is unstable when $\mathbf{x}_1, \mathbf{x}_2$, and \mathbf{x}_3 are nearly parallel to each other (c.f. Remark 6 in Appendix B), which unfortunately is the case for nearly every triangle on a finer triangulation. Another standard approach is to use LU factorization (a.k.a. Gaussian elimination) with partial pivoting (LUPP) [19, p. 114]. In particular, given $\mathbf{A} = [\mathbf{x}_1, \mathbf{x}_2, \mathbf{x}_3]$, one can compute its LUPP

$$\mathbf{P}\mathbf{A} = \mathbf{L}\mathbf{U}, \quad (19)$$

where \mathbf{P} is a permutation matrix corresponding to the row interchanges of \mathbf{A} . Since $\det(\mathbf{P}^T) = \det(\mathbf{P}) = \pm 1$ and $\det(\mathbf{L}) = 1$,

$$\det(\mathbf{A}) = \pm \det(\mathbf{U}) = \pm \prod_{i=1}^3 u_{ii}, \quad (20)$$

where the sign is the same as $\text{sign}(\det(\mathbf{P}))$ and the u_{ii} are the diagonal entries of \mathbf{U} . This technique is more stable than the triple product, but it is still inaccurate when $\mathbf{x}_1, \mathbf{x}_2$, and \mathbf{x}_3 are nearly parallel to each other due to the large condition number of \mathbf{A} . A more sophisticated technique was proposed by Clarkson [20], who adapted modified Gram-Schmidt and used an adaptive procedure to bound relative errors. However, Clarkson's algorithm applies only to integer matrices. To the best of our knowledge, there was no existing method with guaranteed accuracy of the computed determinant with floating-point arithmetic, even for 3×3 matrices.

To achieve accuracy and stability, we notice that

$$\det[\mathbf{x}_1, \mathbf{x}_2, \mathbf{x}_3] = \det[\mathbf{x}_k, \mathbf{x}_{k \oplus 1} - \mathbf{x}_k, \mathbf{x}_{k \oplus 2} - \mathbf{x}_k], \quad (21)$$

where \mathbf{x}_k is chosen to be the vertex incident on the two shorter edges of the triangle $\mathbf{x}_1\mathbf{x}_2\mathbf{x}_3$, and $k \oplus i$ denotes $\text{mod}(k + (i - 1), 3) + 1$. We refer to \mathbf{x}_k as the *anchor*. Note that when $k = 1$, (21) coincides with the triple-product in (14). When $k \neq 1$, shifting the indices as in (21) preserves the determinant. To evaluate the right-hand side of (21), we propose to use (18), which we refer to as *anchored triple product* (or *ATP*), which turns out to be stable in practice. A more sophisticated strategy is to compute (21) using (19–20) with column equilibration [19, p. 139]. In particular, let $\mathbf{A} = [\mathbf{x}_k, \mathbf{x}_{k \oplus 1} - \mathbf{x}_k, \mathbf{x}_{k \oplus 2} - \mathbf{x}_k] \mathbf{D}^{-1}$ with $\mathbf{D} = \text{diag}\{\|\mathbf{x}_k\|, \|\mathbf{x}_{k \oplus 1} - \mathbf{x}_k\|, \|\mathbf{x}_{k \oplus 2} - \mathbf{x}_k\|\}$, and then

$$\det[\mathbf{x}_1, \mathbf{x}_2, \mathbf{x}_3] = \left| \prod_{i=1}^3 d_i u_{ii} \right|. \quad (22)$$

We refer to the latter approach as *anchored LUPP with equilibration* (or *ALUPPE*), and it is even more stable than ATP for some pathological cases.

To justify ATP and ALUPPE, let us first derive error bounds for them for an arbitrary $\mathbf{A} \in \mathbb{R}^{3 \times 3}$. Let $\epsilon_{\text{machine}}$ denote the machine precision, such that $|\text{fl}(x) - x| \leq \epsilon_{\text{machine}}|x|$ and $|\text{fl}(x) \otimes \text{fl}(y)| \leq \epsilon_{\text{machine}}|\text{fl}(x) * \text{fl}(y)|$ for any real value x and y and any basic floating-point \otimes corresponding to a basic arithmetic operator $*$ (such as addition and multiplication), barring overflow and underflow. Let \odot and \otimes denote the inner-product and cross-product operators under floating-point operations.

Theorem 4. *Given \mathbf{A} , let $\tilde{\mathbf{P}}^T \tilde{\mathbf{L}}\tilde{\mathbf{U}}$ be the LUPP of $\mathbf{A}\mathbf{D}^{-1}$ using floating-point arithmetic, where $\mathbf{D} = \text{diag}\{\|\mathbf{a}_1\|, \|\mathbf{a}_2\|, \|\mathbf{a}_3\|\}$. The absolute error of the computed determinant is bounded in the sense that*

$$\left| \prod_{i=1}^3 d_i \tilde{u}_{ii} - \prod_{i=1}^3 d_i u_{ii} \right| = \det(\mathbf{D}) \mathcal{O}(\epsilon_{\text{machine}}). \quad (23)$$

Theorem 5. *Given \mathbf{A} composed of columns \mathbf{a}_1 , \mathbf{a}_2 , and \mathbf{a}_3 , assuming that \mathbf{a}_2 and \mathbf{a}_3 are in counterclockwise order with respect to the direction \mathbf{a}_1 , the absolute error of the computed triple product is bounded in the sense that*

$$|\mathbf{a}_1 \cdot (\mathbf{a}_2 \times \mathbf{a}_3) - \mathbf{a}_1 \odot (\mathbf{a}_2 \otimes \mathbf{a}_3)| = \frac{\det(\mathbf{A})}{\sigma} \mathcal{O}(\epsilon_{\text{machine}}), \quad (24)$$

assuming $\sigma \ll \epsilon_{\text{machine}}$, where $\sigma = |\mathbf{a}_1 \cdot (\mathbf{a}_2 \times \mathbf{a}_3)| / \prod_i \|\mathbf{a}_i\|$.

The proofs of Theorems 4 and 5 involve some detailed backward error analysis. For completeness, we present the proofs in [Appendix A](#) and [Appendix B](#), respectively.

Remark 6. At a high level, $1/\sigma$ in Theorem 5 plays the role of the condition number in computing the cross product. The assumption of $\sigma \gg \epsilon_{\text{machine}}$ in the theorem is for the ease of presentation, because the triple product is nonlinear in \mathbf{A} , so some simplification is required. If σ is close to $\epsilon_{\text{machine}}$, rounding errors would always dominate. Hence, this assumption does not lead to a loss of generality from a practical point of view. As a practical guideline, an accurate and stable algorithm should make σ as large as possible when computing the triple product for a given triangulation.

In the context of computing the Jacobian determinant, we need to substitute \mathbf{x}_k , $\mathbf{x}_{k\oplus 1} - \mathbf{x}_k$, and $\mathbf{x}_{k\oplus 2} - \mathbf{x}_k$ for \mathbf{a}_1 , \mathbf{a}_2 , and \mathbf{a}_3 in the preceding theorems. We can then conclude that $\det(\mathbf{A})$ is proportional to $r_{\text{area}}(\mathbf{x}_1\mathbf{x}_2\mathbf{x}_3)$, so is $\det(\mathbf{D})$, assuming that the minimum angle of the triangle $\mathbf{x}_1\mathbf{x}_2\mathbf{x}_3$ is bounded away from 0. Hence, the relative error of the computed determinant from LUPP is then expected to be $\mathcal{O}(\epsilon_{\text{machine}})$. For ATP, let θ denote the angle between $\mathbf{x}_{k\oplus 1} - \mathbf{x}_k$ and $\mathbf{x}_{k\oplus 2} - \mathbf{x}_k$. Then, σ is proportional to $\sin(\theta)$ for sufficiently small θ , and the assumption $\sigma \gg \epsilon_{\text{machine}}$ is satisfied when θ is bounded away from $\epsilon_{\text{machine}}$. By choosing the anchor \mathbf{x}_k to be the vertex incident on the two shorter edges of the triangle $\mathbf{x}_1\mathbf{x}_2\mathbf{x}_3$, we ensure θ is the maximum angle in the triangle and hence is as close to 90° as possible, so $\det(\mathbf{A})/\det(\mathbf{D})$ and σ are approximately maximized for ALUPPE and ATP, respectively, and they are accurate and stable for almost all practical applications. In contrast, for the naive computation of the triple product in (18), σ is as small as $\sin(\theta_{\min})h^2$, where θ_{\min} is the smallest angle in $\mathbf{x}_1\mathbf{x}_2\mathbf{x}_3$. Hence, a naive computation of the triple product is unstable for small h and small θ_{\min} , and its error is expected to be at least $\mathcal{O}(1/h^2)$ larger than that of ATP.

One shortcoming of the analysis is that it omitted the potential cancellation errors in $\mathbf{x}_{k\oplus 1} - \mathbf{x}_k$ and $\mathbf{x}_{k\oplus 2} - \mathbf{x}_k$. If the spherical triangles are excessively small, these cancellation errors may dominate, and the relative errors from ALUPPE and ATP could be arbitrarily large. Fortunately, the cancellation errors are typically negligible compared to the other errors in practice, even for the finest meshes.

To demonstrate the validity of our analysis, we compare the standard triple product, standard LUPP, and anchored computations for small spherical triangles, along with LUPP with a different vertex as the anchor, which we refer to as “off-anchored.” We generated 1000 random spherical triangles on a unit sphere, of which the longest edge is ~ 0.01 and the shortest edge length is ~ 0.0001 . We applied the algorithms using double-precision floating-point arithmetic and used variable-precision arithmetic with 32-digits of precision to compute the reference solutions. As can be seen from Figure 2, the anchored computations are about six and four orders of magnitude more accurate than the standard triple product and LUPP, respectively. The standard triple product is the least accurate due to its potential reduction of σ by a factor of h^2 compared to ATP. With our choice of anchor, the ATP and ALUPPE have comparable performance. The off-anchored TP is two orders of magnitude worse than ATP due to the reduction of σ by a factor of up to $\sin(\theta_{\min})/\sin(\theta_{\max})$, and similarly for the off-anchored LUPP. ATP has slightly smaller errors than ALUPPE, probably because ATP involves fewer floating-point operators and hence less accumulation of rounding errors. Hence, we use ATP for its better accuracy, efficiency, and simplicity. Note that the mean and minimum errors of ATP are nearly coincident for all cases, indicating that the maximum errors are outliers likely due to near degeneracies (i.e., extremely small triangles). Hence, we expect the errors to be close to machine precision for spherical triangles from practical applications, as we will demonstrate in Section 3.

2.4. Anchored radially projected integration on spheres

We put together the preceding components to obtain an accurate and stable algorithm for numerical integration on a spherical triangle. We refer to the algorithm as *anchored radially projected integration on spherical triangles*, or *ARPIST*. For completeness, Algorithm 1 outlines ARPIST with a given function f . We assumed that the quadrature points $\{\xi_i\}$ and the associated weights $\{w_i\}$ for the reference triangles are pre-tabulated in the procedure, and those rules can be found, for example, in [17] or in the ARPIST GitHub repository. One could replace the function f by an array of its values at the radially projected quadrature points, i.e., $\mathbf{f} = [f(\mathbf{p}(\xi_i))]_i$.

By considering both the truncation and rounding errors, ARPIST can integrate a

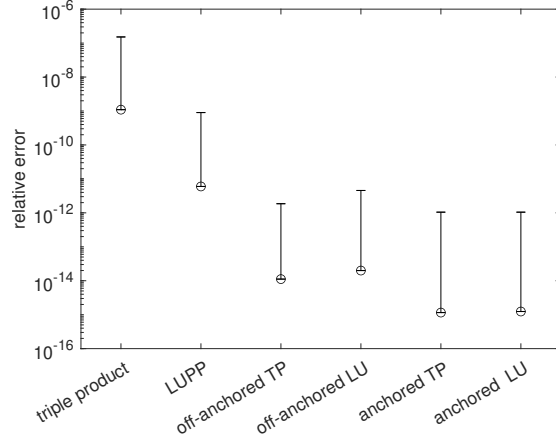


Figure 2: Comparison of different techniques in computing the determinant of random spherical triangles. Circles indicate the mean errors, and the vertical bars indicate the range of the relative errors.

Algorithm 1 Anchored radially projected integration on a spherical triangle

- 1: **procedure** ARPIST($\mathbf{x}_1, \mathbf{x}_2, \mathbf{x}_3, f$) ▷ Integrate f on spherical tri. $\mathbf{x}_1\mathbf{x}_2\mathbf{x}_3$
 - 2: $r \leftarrow \|\mathbf{x}_1\|; t \leftarrow 0$
 - 3: **for** $i = 1$ to npoints **do** ▷ Numerical quadrature over flat tri. $\mathbf{x}_1\mathbf{x}_2\mathbf{x}_3$
 - 4: $\mathbf{x} \leftarrow \mathbf{x}_1 + \xi_i(\mathbf{x}_2 - \mathbf{x}_1) + \eta_i(\mathbf{x}_3 - \mathbf{x}_1)$
 - 5: $t \leftarrow t + w_i f(r\mathbf{x}/\|\mathbf{x}\|)/\|\mathbf{x}\|^3$
 - 6: **end for**
 - 7: $k \leftarrow \arg \min_k \{\|\mathbf{x}_{k\%3+1} - \mathbf{x}_k\| + \|\mathbf{x}_{(k+1)\%3+1} - \mathbf{x}_k\|\}$ ▷ Select anchor
 - 8: **return** $tr^2\mathbf{x}_k \cdot ((\mathbf{x}_{k\%3+1} - \mathbf{x}_k) \times (\mathbf{x}_{(k+1)\%3+1} - \mathbf{x}_k))$ ▷ Scale by $r^2 \det[\mathbf{X}]$
 - 9: **end procedure**
-

sufficiently smooth function stably and accurately, as stated by the following corollary.

Corollary 7. *Given a spherical triangle S with vertices \mathbf{x}_1 , \mathbf{x}_2 , and \mathbf{x}_3 in counter-clockwise order with its corresponding linear triangle T , if the integrand $f(\mathbf{p}) : S \rightarrow \mathbb{R}$ is continuously differentiable to p th order, assuming that $\det(\mathbf{X}) \geq \sigma \|\mathbf{x}_1\| \|\mathbf{x}_2\| \|\mathbf{x}_3\|$ for constant $\sigma \gg \epsilon_{\text{machine}}$, then ARPIST evaluates the spherical integration with a total error of $\text{area}(T)\mathcal{O}(h^{p+1}) + \det(\mathbf{X})/\sigma\mathcal{O}(\epsilon_{\text{machine}})$.*

Corollary 7 directly follows from Theorems 3 and 4. Typically, the truncation errors would dominate, and we expect the integration to approach (near) machine precision for sufficiently smooth functions.

Remark 8. The stability of ARPIST makes it well suited to develop more advanced integration techniques analogous to their counterparts in 1D. For example, we can develop adaptive quadrature rules by recursively subdividing the triangles recursively until the truncation errors are close to machine precision [18, Section 8.3.6], as we will demonstrate in Section 3. As another example, we can apply Romberg integration by leveraging Richardson extrapolation to accelerate convergence [18, Section 8.7].

3. Numerical Experiments

In this section, we report numerical experimentation with ARPIST and compare it with a commonly used technique for computing the areas of spherical triangles [21] and two recently proposed techniques for computing spherical integration [9, 6].

3.1. Accurate and stable computation of spherical-triangle area

We first apply ARPIST to the accurate and stable computation of the area of a spherical triangle, which is mathematically equivalent to the integration of unity, i.e., $f(\mathbf{p}) \equiv 1$. This problem is of particular importance in enforcing global conservation in earth modeling. Hence, it is desirable to be computed as accurately as possible and ideally to (near) machine precision. Presently, this area computation is typically carried out by applying the centuries-old theorems due to Girard and L'Huilier, but such a technique is often observed to be inaccurate. In particular, due to Girard's theorem,

the area of a spherical triangle S with radius R is mathematically equal to $A = R^2 E$, where E is the *spherical excess* of S ; due to L'Huilier's Theorem [21],

$$E = 4 \arctan \sqrt{\tan\left(\frac{s}{2}\right) \tan\left(\frac{s-a_1}{2}\right) \tan\left(\frac{s-a_2}{2}\right) \tan\left(\frac{s-a_3}{2}\right)}, \quad (25)$$

where the a_i are the length of sides on the spherical triangle and $s = (a_1 + a_2 + a_3)/2$ is the semiperimeter of S . Since (25) is the core of this computation, we refer to the approach as L'Huilier's theorem or *LT*. Due to its popularity, we will use LT as the baseline in assessing ARPIST for this problem. As a side product, we will reveal the numerical instabilities in LT that have led to the inaccuracy of this popular technique.

For the area computation to be accurate and stable, it needs to be insensitive to the sizes and shapes of the triangles. More precisely, it should be stable when the maximum edge length h or the minimum angle θ_{\min} tends to 0 (or tends to $\epsilon_{\text{machine}}^\alpha$ for some $0.5 \lesssim \alpha < 1$ so that rounding errors would not dominate truncation errors). We assess the accuracy of ARPIST using double-precision arithmetic as h or θ_{\min} tends to zero in Figure 3. We computed the reference solution using (25) with 128-digits quadruple-precision floating-point numbers. For ARPIST, we report the results using degree-4 and degree-8 quadrature rules. In addition, we report the results for an adaptive procedure as we alluded to in Remark 8. The adaptive ARPIST applies degree-4 and degree-8 Gaussian quadrature rules if $h \leq h_1$ and $h_1 < h \leq h_2$, respectively, and recursively splits a larger triangle if $h > h_2$, where h_1 and h_2 are determined experimentally. Figure 3(a) shows the relative errors in computed areas of spherical triangles on a unit sphere for $\pi/500 \leq \theta_{\min} \leq \pi/3$, where $h \approx 0.26$. It can be seen that degree-4, degree-8, and adaptive ARPIST are all insensitive to θ_{\min} . Figure 3(b) shows the errors for equilateral triangles with $10^{-3} \leq h \leq 1$. It is clear that degree-4 and degree-8 ARPIST achieved near machine precision (below 10^{-15}) for $h \lesssim 0.004$ and $h \lesssim 0.05$, respectively. Hence, we set $h_1 = 0.004$ and $h_2 = 0.05$ in adaptive ARPIST.

In Figure 3, it is also evident that the relative errors in LT increased steadily as θ_{\min} or h decreased. Despite its remarkably accuracy for $h \approx 1$, the errors of LT reached about 10^{-10} for poorly shaped large triangles in Figure 3(a) and 10^{-7} for poorly shaped small triangles. The poor accuracy of LT for poor-shaped triangles is

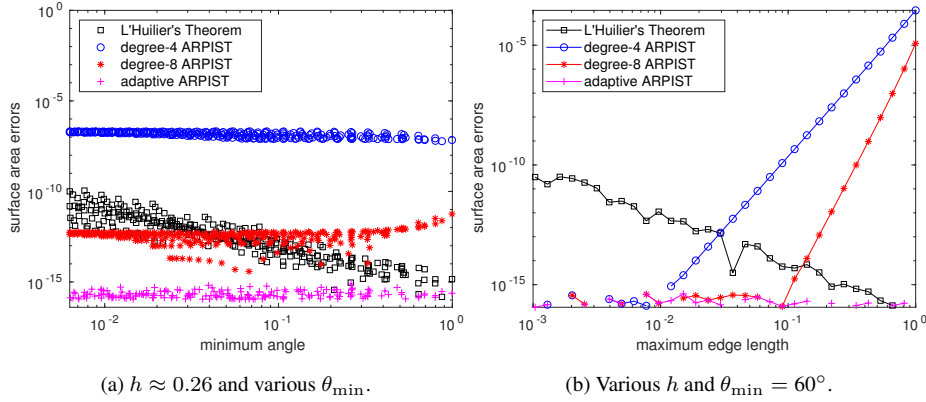


Figure 3: Relative errors of computed areas of spherical triangles using ARPIS T versus L'Huilier's Theorem in double precision for isosceles triangles with various minimum angles and edge lengths. In (a), the errors of ARPIS T do not change much for spherical triangles with different minimum angles, while the errors of the L'Huilier's Theorem increase as the minimum angles decrease. In (b), the errors of degree-4 and degree-8 ARPIS T decrease as the maximum edge length decrease until they reach the machine precision, while the errors of the L'Huilier's Theorem increase as the maximum edge lengths decrease.

due to the cancellation errors in $s - a_i$ in (25), which are catastrophic when θ_{\min} is close to 0. The instability of LT for small well-shaped triangles, on the other hand, is due to the astronomical (absolute) condition number of the square-root operation, i.e.,

$$\kappa(\sqrt{x}) = \limsup_{\epsilon \rightarrow 0} \frac{|\sqrt{x+\epsilon} - \sqrt{x}|}{|\epsilon|} = \frac{d\sqrt{x}}{dx} = \frac{1}{2\sqrt{x}}, \quad (26)$$

which tends to ∞ as x approaches 0. As h approaches 0, the operand of the square-root operation in (25) tends to 0 because $s/2$, $(s - a_i)/2$, and their tangents all tend to 0. Hence, this condition number in (26) drastically amplifies the rounding and cancellation errors, leading to large errors for LT as seen in Figure 3. Hence, LT is unstable for fine meshes even with well-shaped triangles, but it is particularly disastrous for those with poor-shaped small triangles. To the best of our knowledge, adaptive ARPIS T offers the first viable alternative for general meshes to achieve (near) machine precision for computing spherical-triangle areas, as long as h and θ_{\min} are sufficiently large relative to $\epsilon_{\text{machine}}$.

3.2. Integration of smooth analytic functions

To assess the accuracy and efficiency of ARPIST for integrating smooth analytic function on spheres, we compare it with two techniques, namely LSQST [9] and SQRBF [6, 12]. We chose these two techniques for comparison because they can be applied to any given triangulation of a sphere and they were developed recently.

3.2.1. Comparison with LSQST

We first compare ARPIST with LSQST. The source code of LSQST is unavailable, and its algorithm is very difficult to implement, so we applied the adaptive ARPIST to solve a representative test problem as described in Section 2.2 of [9]. In particular, we integrate the test function

$$f^{(q,s)}(\mathbf{x}) = \sum_{l=1}^9 \alpha_l^{(q)} G_s \left(\left\langle \mathbf{x}, \boldsymbol{\eta}_l^{(q)} \right\rangle_2 \right), \quad (27)$$

where the coefficients $\alpha_l^{(q)}$ and the centers $\boldsymbol{\eta}_l^{(q)}$ are randomly chosen, and

$$G_s(t) = \frac{(1-s)^3}{(1-2st+s^2)^{3/2}}$$

is the Poisson kernel for some $s \in [0, 1)$.¹ We chose the parameters

$$s = 0.8, 0.9, 0.95, 0.97, 0.975, 0.98, 0.985, 0.99, 0.995,$$

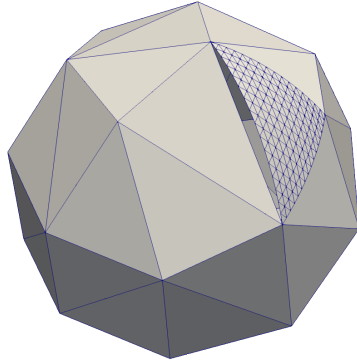
which is a subset of those in [9]. We excluded the two cases $s = 0.999$ and $s = 0.9999$, since $G_s(t)$ tends to a discontinuous function as s approaches 1 and robust resolution of discontinuities is a separate topic in its own right (see, e.g., [22]). As in [9], we compute the average errors for 50 random pairs $(\alpha_l^{(q)}, \boldsymbol{\eta}_l^{(q)})$,

$$E(s) = \frac{1}{50} \sum_{q=1}^{50} \frac{|I_{\mathbb{S}^2}(f^{(q,s)}) - Q_{\mathbb{S}^2}(f^{(q,s)})|}{|I_{\mathbb{S}^2}(f^{(q,s)})|},$$

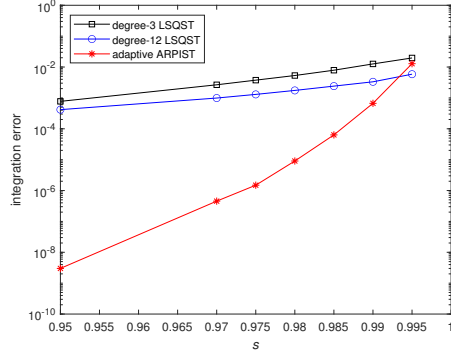
where

$$I_{\mathbb{S}^2}(f^{(q,s)}) = \int_{\mathbb{S}^2} f^{(q,s)} \left(\left\langle \mathbf{x}, \boldsymbol{\eta}_l^{(q)} \right\rangle_2 \right) d\mu(x) = 4\pi \frac{(1-s)^2}{1+s}$$

¹In [9], the authors used h instead of s . We use s to avoid the confusion with edge length.



(a) Test mesh as used in [9].



(b) Integration errors for different s .

Figure 4: Average quadrature errors $E(s)$ by integrating $f^{(q,s)}$ in (27) for different s on the test mesh.

and $Q_{\mathbb{S}^2}(f^{(q,s)})$ is the numerical integration of $f^{(q,s)}$ using ARPIST or LSQST. As in [9], we generated a triangular mesh with 60 triangles using STRIPACK [23] and then split one of the triangles into 256 small triangles as shown in Figure 4(a). We applied the adaptive ARPIST as described in Section 3.1 on this test mesh, resulting in 786,432 quadrature points.

As shown in Figure 4(b), the error $E(s)$ for ARPIST ranged between 3×10^{-9} and 1.28×10^{-2} as s increased. As points of reference, Figure 4(b) reproduced the two representative results of degree-3 and degree-12 LSQST from Figure 2 of [9] with 1,944,000 quadrature points. It can be seen that the errors from ARPIST are about an order of magnitude smaller than LSQST for $s = 0.99$. The performance gap increased drastically as s increased, and ARPIST outperformed LSQST by five orders of magnitude for $s = 0.95$. Remarkably, ARPIST achieved this drastic improvement of accuracy with a much simpler algorithm. The runtimes of LSQST were not reported in [9]. We estimate that ARPIST is at least an order of magnitude faster because the computational costs of ARPIST and LSQST are linear and superlinear in the number of quadrature points within each triangle, respectively.

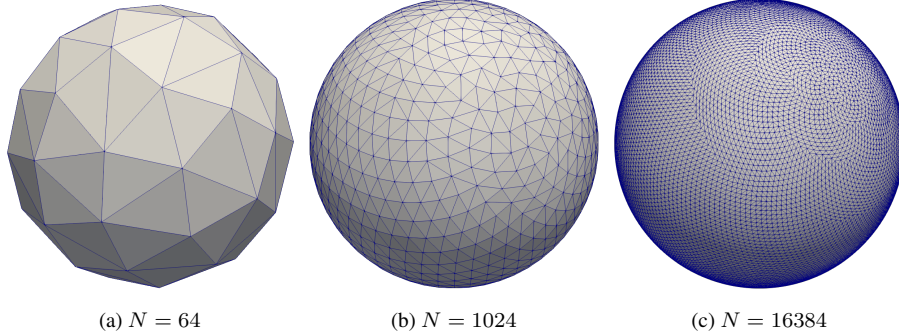


Figure 5: Three representative test meshes in the comparison between ARPIST and SQRBF.

3.2.2. Comparison with SQRBF

In this test, we compare ARPIST with the RBF-based spherical quadrature, or SQRBF [6]. Since SQRBF has an open-source MATLAB implementation [12], we could conduct a more in-depth comparison on a range of meshes. In particular, we used STRIPACK [23] to generate a series of six Delaunay triangulations of the unit sphere with $N = 4^{2+i}$ nodes for $i = 1, 2, \dots, 6$. Figure 5 shows three representative meshes. For ARPIST, we focused on degree-4 and degree-8 Gaussian quadrature rules on each triangle, which have 6 and 16 quadrature points per triangle, respectively. Hence, the total numbers of quadrature points on the whole sphere are $12(4^i - 2)$ and $32(4^i - 2)$ for the i th mesh. For each technique, the integration of any smooth function over the whole sphere is then a weighted sum of the function values at the quadrature points. We compared the three techniques for several test functions in [6], and the results were qualitatively the same. Hence, we present only the result for one of the test functions,

$$f_1(x, y, z) = \frac{1}{9}(1 + \tanh(9(z - x - y))), \quad (28)$$

of which the exact integral over the sphere is $I_{\mathbb{S}^2}(f_1) = 4\pi/9$.

In Figure 6, we compare ARPIST with SQRBF in terms of accuracy and efficiency. Note that the different methods have different numbers of quadrature points. Figures 6(a) and (b) show the relative integration errors with respect to the numbers of quadrature points and the numbers of elements, respectively. It can be seen that

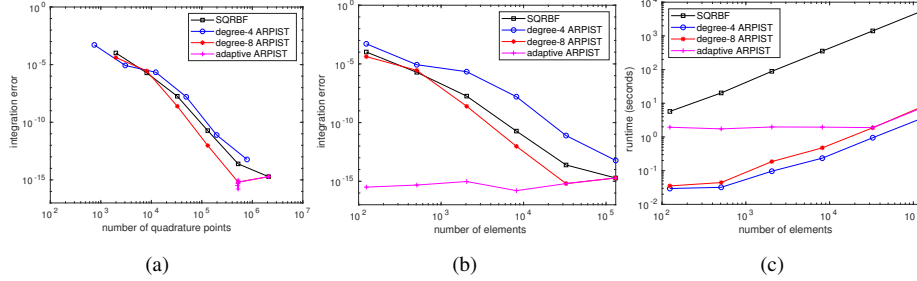


Figure 6: Comparison of errors and runtimes between ARPIST and SQRBF.

degree-8 ARPIST delivered better accuracy than SQRBF while SQRBF was more accurate than degree-4 ARPIST. For completeness, we also report the results for adaptive ARPIST, which achieved near machine precision for all the meshes because its adaptive procedure generated roughly the same numbers of quadrature points for coarser meshes. In Figure 6(c), we compare the computational costs of the MATLAB implementations of ARPIST and SQRBF. Both degree-4 and degree-8 ARPIST were about three orders of magnitude faster than SQRBF. The adaptive ARPIST was also more efficient than SQRBF, but it was less efficient than fixed-degree ARPIST for coarser meshes. The cost of adaptive ARPIST can be further reduced by enlarging its thresholds h_1 and h_2 for splitting the triangles to reduce the number of quadrature points if lower-precision solutions are needed. Hence, we conclude that ARPIST is much more accurate, efficient, and robust than SQRBF. It is worth noting that ARPIST is also much easier to implement, for example, in C++, to achieve even greater performance. More importantly, ARPIST is more flexible than SQRBF because it can be applied to individual triangles while SQRBF only applies to a whole spherical triangulation.

3.3. Comparison for scattered data

Our preceding examples consider analytical functions. In practice, an analytic function may not be available and the function values may be sampled at some given scattered data points, such as the nodes of a given triangulation. The latter is the main assumption in LSQST and SQRBF. Mathematically, it simply means that we must reconstruct the values at the quadrature points from the scattered data values using an

interpolation or quasi-interpolation with comparable accuracy to the quadrature rules. In the context of ARPIST, it can be achieved by using a weighted-least-squares (WLS) reconstruction, similar to that in [24]. We omit the details of WLS and refer readers to our previous works in [24], [25], or [22] for details. For completeness, we briefly describe how to couple WLS with ARPIST.

Suppose the function f is sampled at discrete points $\{\mathbf{x}_k\}_{k=1}^n$, and let $f_k = f(\mathbf{x}_k)$. To compute the integration over a given triangle e_i on a sphere, we first use ARPIST to generate the quadrature points $\{\mathbf{x}_{ij} \mid 1 \leq j \leq \ell_i\}$ and corresponding weights $\{w_{ij}\}$ in the triangle. Then, we use WLS reconstruction to compute a sparse operator $\mathbf{A}_i \in \mathbb{R}^{\ell_i \times n}$ to interpolate the function values from the scattered points $\{\mathbf{x}_k\}_{k=1}^n$ to the quadrature points $\{\mathbf{x}_{ij}\}$. The spherical integration operator over the triangle is

$$\mathbf{b}_i^T = \mathbf{w}_i^T \mathbf{A}_i,$$

where $\mathbf{w}_i \in \mathbb{R}^{\ell_i}$ is a column vector composed of w_{ij} and $\mathbf{b}_i \in \mathbb{R}^n$. Given a column vector $\mathbf{f} = (f_1, f_2, \dots, f_n)^T$, the integral over e_i is simply $\mathbf{b}_i^T \mathbf{f}$. To obtain an integration operator over the complete triangulation, one simply needs to add up \mathbf{b}_i for all the triangles $\{e_i \mid 1 \leq i \leq m\}$, i.e., $\mathbf{b} = \sum \mathbf{b}_i$. Then, $\mathbf{b}^T \mathbf{f}$ is the total integral over the whole sphere.

To assess the accuracy of ARPIST+WLS,² we compare it with SQRBF for two test functions in [6], namely f_1 in (28) and

$$f_2(x, y, z) = \frac{1}{2} + \frac{\arctan(300(z - 0.9999))}{\pi}.$$

The exact integral of f_2 over the sphere is $I_{\mathbb{S}^2}(f_2) \approx 0.014830900415995262852$ [26]. We used STRIPACK [23] to generate a series of Delaunay triangulations of the unit sphere with $N = 4^{4+i}$ nodes for $i = 1, 2, \dots, 5$ and then sampled the functions at the nodes of the triangulations. Since SQRBF can only integrate over the whole sphere, we computed the operator \mathbf{b} in ARPIST+WLS instead of \mathbf{b}_i for the individual triangles. Since ARPIST uses degree-4 and degree-8 quadrature rules, we used degree-4, degree-6, and degree-8 WLS to match the accuracy of the quadrature rules. As can be seen

²We are unable to compare with LSQST for this test due to the unavailability of its source code.

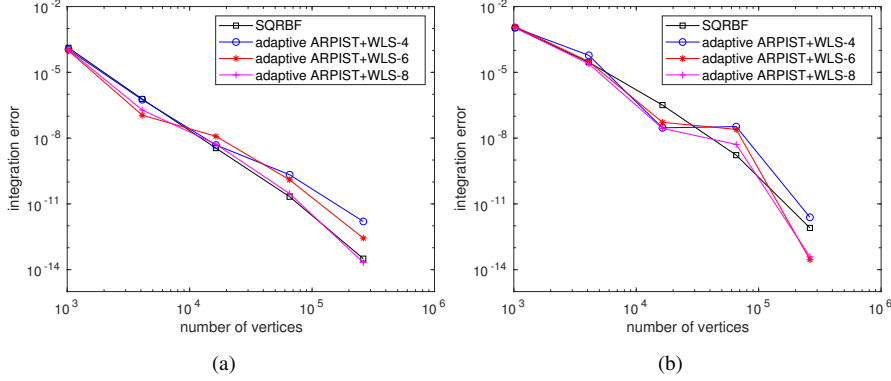


Figure 7: Comparison of overall integration errors between ARPIST+WLS and SQRBF.

in Figure 7, ARPIST with degree-8 WLS is comparable with SQRBF for f_1 , and it outperformed SQRBF on most of the meshes for f_2 . However, ARPIST with degree-4 and degree-6 WLS under-performed both SQRBF and ARPIST+WLS-8 for finer meshes, because their interpolation errors dominated the integration errors. It is worth noting that SQRBF uses higher-degree polynomials than WLS-8, and it is designed for integrating over the whole sphere only.

4. Conclusions

In this work, we propose a new integration technique for spherical triangles, called ARPIST. ARPIST utilizes a simple and effective transformation from the spherical triangle to the linear triangle via radial projection to achieve high accuracy and efficiency. More importantly, ARPIST overcomes the potential instabilities in the Jacobian determinant of the transformation to achieve provable accuracy and stability even for poorly shaped triangles. Our experimental results verified that ARPIST could reliably achieve (near) machine precision. We also showed that ARPIST is orders of magnitude more accurate than the popular technique of computing the area of spherical triangles based on L’Huilier’s Theorem. ARPIST is also more accurate and significantly more efficient than other recently proposed techniques for integrating smooth functions on spheres. When coupled with degree-8 WLS reconstructions, ARPIST can integrate scattered

data values with similar or better accuracy compared to SQRBF. One limitation of this work is that it considered only smooth functions. In addition, if the function has discontinuities, then using a high-degree quadrature rule would generally lead to instabilities due to the violation of the regularity assumptions of high-degree quadrature rules. Some high-order limiters (such as WLS-ENO [22]) are needed in this setting. We plan to address this issue in the future.

Acknowledgments

This work was supported under the Scientific Discovery through Advanced Computing (SciDAC) program in the US Department of Energy's Office of Science, Office of Advanced Scientific Computing Research through subcontract #462974 with Los Alamos National Laboratory. We thank Drs. Vijay S. Mahadevan and Paul Ullrich for helpful discussions on spherical integration, which have motivated this work, and thank Dr. Qiao Chen for his help in proofreading the paper. We thank the anonymous reviewers for their helpful comments.

References

- [1] A. McLaren, Optimal numerical integration on a sphere, *Math. Comput.* 17 (84) (1963) 361–383.
- [2] V. I. Lebedev, Quadratures on a sphere, *USSR Computational Mathematics and Mathematical Physics* 16 (2) (1976) 10–24.
- [3] K. Atkinson, W. Han, Spherical harmonics and approximations on the unit sphere: an introduction, Vol. 2044, Springer Science & Business Media, 2012.
- [4] F. Dai, Y. Xu, Approximation theory and harmonic analysis on spheres and balls, Vol. 23, Springer, 2013.
- [5] K. Hesse, I. H. Sloan, R. S. Womersley, Numerical integration on the sphere, in: W. Freeden, M. Z. Nashed, T. Sonar (Eds.), *Handbook of Geomathematics*, 2nd Edition, 2015, pp. 2671–2710.

- [6] J. A. Reeger, B. Fornberg, Numerical quadrature over the surface of a sphere, *Stud. Appl. Math.* 137 (2) (2016) 174–188.
- [7] B. Portelenelle, J.-P. Croisille, An efficient quadrature rule on the cubed sphere, *J. Comput. Appl. Math.* 328 (2018) 59–74.
- [8] K. Atkinson, Numerical integration on the sphere, *ANZIAM J.* 23 (3) (1982) 332–347.
- [9] J. Beckmann, H. Mhaskar, J. Prestin, Local numerical integration on the sphere, *GEM - Int. J. Geomath.* 5 (2) (2014) 143–162.
- [10] A. Sommariva, M. Vianello, Near-algebraic tchakaloff-like quadrature on spherical triangles, *Applied Mathematics Letters* 120 (2021) 107282.
- [11] A. Sommariva, M. Vianello, Numerical hyperinterpolation over spherical triangles, *Mathematics and Computers in Simulation* 190 (2021) 15–22.
- [12] J. A. Reeger, Spherical_Quadrature_RBF (Quadrature_Nodes), https://www.mathworks.com/matlabcentral/fileexchange/51214-spherical_quadrature_rbf-quadrature_nodes, MATLAB Central File Exchange. Retrieved December 4, 2021 (2015).
- [13] P. A. Ullrich, D. Devendran, H. Johansen, Arbitrary-order conservative and consistent remapping and a theory of linear maps: Part ii, *Mon. Weather Rev.* 144 (4) (2016) 1529–1549.
- [14] J. P. Snyder, *Map Projections—A Working Manual*, Vol. 1395, US Government Printing Office, 1987.
- [15] J. Humpherys, T. J. Jarvis, E. J. Evans, *Foundations of Applied Mathematics, Volume I: Mathematical Analysis*, SIAM, 2017.
- [16] T.-W. Ma, Higher chain formula proved by combinatorics, *Electron. J. Comb.* 16 (1) (2009) N21. doi:10.37236/259.

- [17] R. Cools, An encyclopedia of cubature formulas, *J. Complex.* 19 (3) (2003) 445–453.
- [18] M. T. Heath, *Scientific Computing: An Introductory Survey*, Revised Second Edition, SIAM, 2018.
- [19] G. H. Golub, C. F. Van Loan, *Matrix Computations*, 4th Edition, Johns Hopkins, 2013.
- [20] K. L. Clarkson, Safe and effective determinant evaluation, *IEEE Foundations of Computer Science* 33 (1992) 387–395.
- [21] W. H. Beyer, *CRC standard mathematical tables and formulae*, 28th Edition, Boca Raton, FL: CRC Press, 1987.
- [22] Y. Li, Q. Chen, X. Wang, X. Jiao, WLS-ENO remap: Superconvergent and non-oscillatory weighted least squares data transfer on surfaces, *J. Comput. Phys.* 417 (2020) 109578.
- [23] R. J. Renka, Algorithm 772: STRIPACK: Delaunay triangulation and Voronoi diagram on the surface of a sphere, *ACM Trans. Math. Software* 23 (3) (1997) 416–434.
- [24] N. Ray, D. Wang, X. Jiao, J. Glimm, High-order numerical integration over discrete surfaces, *SIAM J. Numer. Ana.* 50 (2012) 3061–3083.
- [25] Y. Li, X. Zhao, N. Ray, X. Jiao, Compact feature-aware hermite-style high-order surface reconstruction, *Engineering with Computers* (2019) 1–24.
- [26] E. Fuselier, T. Hangelbroek, F. J. Narcowich, J. D. Ward, G. B. Wright, Kernel based quadrature on spheres and other homogeneous spaces, *Numerische Mathematik* 127 (1) (2014) 57–92.
- [27] L. N. Trefethen, D. Bau III, *Numerical Linear Algebra*, Vol. 50, SIAM, 1997.

Appendix A. Error analysis of LUPP with equilibration

We prove the error bounds of the determinant using LUPP in Theorem 4 by adapting the standard backward error analysis in linear algebra.

Proof. Without loss of generality, assume \mathbf{a}_2 and \mathbf{a}_3 are in counterclockwise order w.r.t. \mathbf{a}_1 , so that $\det(\mathbf{A}) > 0$. First, consider the equilibrated matrix $\mathbf{B} = \mathbf{A}\mathbf{D}^{-1}$. Let $\tilde{\mathbf{P}}\mathbf{B} = \tilde{\mathbf{L}}\tilde{\mathbf{U}}$ be the LUPP with floating-point arithmetic. We claim that the computed determinant is backward stable in the sense that there exists $\tilde{\mathbf{B}} = [\tilde{\mathbf{b}}_1, \tilde{\mathbf{b}}_2, \tilde{\mathbf{b}}_3]$ with $\|\tilde{\mathbf{b}}_i - \mathbf{b}_i\| = \mathcal{O}(\epsilon_{\text{machine}})\|\mathbf{b}_i\| = \mathcal{O}(\epsilon_{\text{machine}})$ for $i = 1, 2, 3$ such that

$$\left| \det(\tilde{\mathbf{B}}) \right| = \left| \prod_{i=1}^3 \tilde{u}_{ii} \right|.$$

This backward stability follows from the classical backward error analysis of LUPP [27, Theorem 22.2]: There exists $\tilde{\mathbf{B}} = [\tilde{\mathbf{b}}_1, \tilde{\mathbf{b}}_2, \tilde{\mathbf{b}}_3]$ with $\|\tilde{\mathbf{B}} - \mathbf{B}\|_\infty = \|\mathbf{B}\|_\infty \mathcal{O}(\epsilon_{\text{machine}})$ for $i = 1, 2, 3$, such that $\tilde{\mathbf{P}}\tilde{\mathbf{B}} = \tilde{\mathbf{L}}\tilde{\mathbf{U}}$, where $\tilde{\mathbf{L}}$ is unit lower triangular (i.e., with ones along its diagonal), and $\tilde{\mathbf{P}}$ is another permutation matrix. Hence, $\left| \det(\tilde{\mathbf{B}}) \right| = \left| \det(\tilde{\mathbf{U}}) \right| = \left| \prod_{i=1}^3 \tilde{u}_{ii} \right|$. Furthermore, under the assumption of $\|\mathbf{b}_i\| = 1$, $1 \leq \|\mathbf{B}\| \leq \sqrt{3}$, so $\|\tilde{\mathbf{b}}_i - \mathbf{b}_i\| \leq \|\tilde{\mathbf{B}} - \mathbf{B}\| = \mathcal{O}(\epsilon_{\text{machine}})$.

Second, the absolute condition number of $\det(\mathbf{B})$ w.r.t. perturbations in b_{ij} is $\left| \frac{\partial \det(\mathbf{B})}{\partial b_{ij}} \right| = |\det(\mathbf{B}_{ij})|$, where \mathbf{B}_{ij} denotes the 2-by-2 matrix obtained by removing the i th row and j th column in \mathbf{B} . The absolute condition number of $\det(\mathbf{B})$ in ∞ -norm is $\kappa_{\det} = \left\| \left[\frac{\partial \det(\mathbf{B})}{\partial b_{ij}} \right]_{ij} \right\|_\infty$, and

$$\left| \det(\tilde{\mathbf{B}}) - \det(\mathbf{B}) \right| \leq \kappa_{\det} \|\tilde{\mathbf{B}} - \mathbf{B}\|_\infty = \kappa_{\det} \|\mathbf{B}\|_\infty \mathcal{O}(\epsilon_{\text{machine}}). \quad (\text{A.1})$$

Given that \mathbf{B} is equilibrated, $\kappa_{\det} \leq 6$ and $\|\mathbf{B}\|_\infty \leq 3$, so $\left| \left| \det(\tilde{\mathbf{B}}) \right| - \left| \det(\mathbf{B}) \right| \right| \leq \left| \det(\tilde{\mathbf{B}}) - \det(\mathbf{B}) \right| = \mathcal{O}(\epsilon_{\text{machine}})$.

Finally, let \tilde{d}_i be $\|\mathbf{a}_i\|$ computed in floating-point arithmetic.

$$\det(\tilde{\mathbf{D}}) = \prod_i \tilde{d}_i = (1 + \mathcal{O}(\epsilon_{\text{machine}})) \det(\mathbf{D}).$$

Therefore,

$$\begin{aligned}
& \left| \left| \prod_{i=1}^3 d_i \tilde{u}_{ii} \right| - \left| \prod_{i=1}^3 d_i u_{ii} \right| \right| \\
& \leq \left| \prod_{i=1}^3 d_i \tilde{u}_{ii} - \prod_{i=1}^3 d_i u_{ii} \right| \\
& = \left| \det(\tilde{\mathbf{D}}) \det(\tilde{\mathbf{B}}) - \det(\mathbf{D}) \det(\mathbf{B}) \right| \\
& = \left| \det(\tilde{\mathbf{D}}) \det(\tilde{\mathbf{B}}) - \det(\mathbf{D}) \det(\tilde{\mathbf{B}}) + \det(\mathbf{D}) \det(\tilde{\mathbf{B}}) - \det(\mathbf{D}) \det(\mathbf{B}) \right| \\
& \leq \det(\tilde{\mathbf{B}}) \left| \det(\tilde{\mathbf{D}}) - \det(\mathbf{D}) \right| + \det(\mathbf{D}) \left| \det(\tilde{\mathbf{B}}) - \det(\mathbf{B}) \right| \\
& = \det(\mathbf{D}) \mathcal{O}(\epsilon_{\text{machine}}).
\end{aligned}$$

□

In the proof, column equilibration played an important role. Without equilibration, it would be more difficult to bound $\kappa_{\det} \|\mathbf{B}\|_{\infty}$ in (A.1). Nevertheless, LUPP without equilibration turned out to perform well in practice.

Appendix B. Error analysis of anchored triple product

We now generalize the error analysis in Appendix A to prove Theorem 5 for ATP. The algorithm for ATP is simpler, but its analysis needs to deviate from the standard backward error analysis. To this end, we define $\sigma := |\mathbf{a} \cdot (\mathbf{b} \times \mathbf{c})| / \|\mathbf{a}\| \|\mathbf{b}\| \|\mathbf{c}\|$, so that $1/\sigma$ will play the role of the *relative condition number* under the assumption that $\sigma \gg \epsilon_{\text{machine}}$. This simplification is necessary because the triple product is a nonlinear (quadratic) operation, so unlike in linear algebra, one cannot give a simple closed form for the condition number when $\sigma \approx \epsilon_{\text{machine}}$.

Proof. We first show that the relative error in the triple product $\mathbf{a} \cdot (\mathbf{b} \times \mathbf{c})$ is approximately bounded by $\mathcal{O}(\epsilon_{\text{machine}})/\sigma$ when $\sigma \gg \epsilon_{\text{machine}}$. Without loss of generality,

assume that a_i , b_i , and c_i are all floating-point numbers. Then,

$$\begin{aligned} \mathbf{b} \otimes \mathbf{c} &= \begin{bmatrix} (b_2 c_3 (1 + \epsilon_1) - b_3 c_2 (1 + \epsilon_2)) (1 + \epsilon_7) \\ (b_3 c_1 (1 + \epsilon_3) - b_1 c_3 (1 + \epsilon_4)) (1 + \epsilon_8) \\ (b_1 c_2 (1 + \epsilon_5) - b_2 c_1 (1 + \epsilon_6)) (1 + \epsilon_9) \end{bmatrix} \\ &= \begin{bmatrix} b_2 c_3 (1 + \epsilon'_2) - b_3 c_2 (1 + \epsilon'_6) \\ b_3 c_1 (1 + \epsilon'_3) - b_1 c_3 (1 + \epsilon'_4) \\ b_1 c_2 (1 + \epsilon'_1) - b_2 c_1 (1 + \epsilon'_5) \end{bmatrix}, \end{aligned}$$

where $|\epsilon_i| \leq \epsilon_{\text{machine}}$ and $|\epsilon'_i| \leq 2\epsilon_{\text{machine}} + \mathcal{O}(\epsilon_{\text{machine}}^2)$. Let $\tilde{\mathbf{v}}$ denote $\mathbf{b} \otimes \mathbf{c}$. Then,

$$\begin{aligned} \mathbf{a} \odot (\mathbf{b} \otimes \mathbf{c}) &= ((a_1(1 + \epsilon_{10})\tilde{v}_1 + a_2(1 + \epsilon_{11})\tilde{v}_2) (1 + \epsilon_{12}) + a_3(1 + \epsilon_{13})\tilde{v}_3) (1 + \epsilon_{14}) \\ &= (a_1(1 + \epsilon_{a1})) \tilde{v}_1 + (a_2(1 + \epsilon_{a2})) \tilde{v}_2 + (a_3(1 + \epsilon_{a3})) \tilde{v}_3 \end{aligned}$$

where $|\epsilon_{ai}| \leq 3\epsilon_{\text{machine}} + \mathcal{O}(\epsilon_{\text{machine}}^2)$ for $1 \leq i \leq 2$ and $|\epsilon_{a3}| \leq 2\epsilon_{\text{machine}} + \mathcal{O}(\epsilon_{\text{machine}}^2)$.

Let $\tilde{\mathbf{a}} = [a_i(1 + \epsilon_{ai})]_i$ and $\tilde{\mathbf{b}} = [b_i(1 + \epsilon'_i)]_i$ for $1 \leq i \leq 3$, and then

$$\begin{aligned} \mathbf{a} \odot (\mathbf{b} \otimes \mathbf{c}) - \tilde{\mathbf{a}} \cdot (\tilde{\mathbf{b}} \times \mathbf{c}) &= \tilde{\mathbf{a}} \cdot (\tilde{\mathbf{b}} \times \mathbf{c}) - \tilde{\mathbf{a}} \cdot \begin{bmatrix} \tilde{b}_2 c_3 - \tilde{b}_3 c_2 \frac{1 + \epsilon'_6}{1 + \epsilon'_3} \\ \tilde{b}_3 c_1 - \tilde{b}_1 c_3 \frac{1 + \epsilon'_4}{1 + \epsilon'_1} \\ \tilde{b}_1 c_2 - \tilde{b}_2 c_1 \frac{1 + \epsilon'_5}{1 + \epsilon'_2} \end{bmatrix} \\ &= \tilde{a}_1 \tilde{b}_3 c_2 \epsilon''_1 + \tilde{a}_2 \tilde{b}_1 c_3 \epsilon''_2 + \tilde{a}_3 \tilde{b}_2 c_1 \epsilon''_3, \end{aligned} \quad (\text{B.1})$$

where $|\epsilon''_i| \leq 4\epsilon_{\text{machine}} + \mathcal{O}(\epsilon_{\text{machine}}^2)$. Assuming $\sigma \gg \epsilon_{\text{machine}}$, it is easy to show that

$$\left\| \tilde{\mathbf{a}} \cdot (\tilde{\mathbf{b}} \times \mathbf{c}) \right\| \geq \tilde{\sigma} \|\tilde{\mathbf{a}}\| \|\tilde{\mathbf{b}}\| \|\mathbf{c}\|,$$

where $\tilde{\sigma} = \sigma(1 + \mathcal{O}(\epsilon_{\text{machine}}))$, and

$$\begin{aligned} \left| \tilde{a}_1 \tilde{b}_3 c_2 \epsilon''_1 + \tilde{a}_2 \tilde{b}_1 c_3 \epsilon''_2 + \tilde{a}_3 \tilde{b}_2 c_1 \epsilon''_3 \right| &\leq \|\tilde{\mathbf{a}}\| \|\tilde{\mathbf{b}}\| \|\mathbf{c}\| \mathcal{O}(\epsilon_{\text{machine}}) \\ &\leq \frac{1}{\tilde{\sigma}} \left\| \tilde{\mathbf{a}} \cdot (\tilde{\mathbf{b}} \times \mathbf{c}) \right\| \mathcal{O}(\epsilon_{\text{machine}}) \\ &= \frac{1}{\sigma} \left\| \tilde{\mathbf{a}} \cdot (\tilde{\mathbf{b}} \times \mathbf{c}) \right\| \mathcal{O}(\epsilon_{\text{machine}}). \end{aligned}$$

If the input numbers were not yet floating-point numbers, we only need to increase the constant factors for the ϵ , and the asymptotic argument still holds.

Second, substituting \mathbf{a}_1 , \mathbf{a}_2 , and \mathbf{a}_3 for \mathbf{a} , \mathbf{b} , and \mathbf{c} in the above, and following a similar argument as for ALUPPE in [Appendix A](#), we obtain

$$\begin{aligned} |\mathbf{a}_1 \cdot (\mathbf{a}_2 \times \mathbf{a}_3) - \tilde{\mathbf{a}}_1 \cdot (\tilde{\mathbf{a}}_2 \times \mathbf{a}_3)| &= \prod_i \|\mathbf{a}_i\| \mathcal{O}(\epsilon_{\text{machine}}) \\ &\leq \frac{1}{\sigma} \det(\mathbf{A}) \mathcal{O}(\epsilon_{\text{machine}}) \end{aligned}$$

under the assumptions that \mathbf{a}_2 and \mathbf{a}_3 are in counterclockwise order with respect to \mathbf{a}_1 and that $|\mathbf{a}_1 \cdot (\mathbf{a}_2 \times \mathbf{a}_3)| \geq \sigma \prod_i \|\mathbf{a}_i\|$ for constant $\sigma \gg \epsilon_{\text{machine}}$. Similarly,

$$|\mathbf{a}_1 \odot (\mathbf{a}_2 \otimes \mathbf{a}_3) - \tilde{\mathbf{a}}_1 \cdot (\tilde{\mathbf{a}}_2 \times \mathbf{a}_3)| \leq \frac{1}{\sigma} \det(\mathbf{A}) \mathcal{O}(\epsilon_{\text{machine}}).$$

Hence,

$$\begin{aligned} &|\mathbf{a}_1 \cdot (\mathbf{a}_2 \times \mathbf{a}_3) - \mathbf{a}_1 \odot (\mathbf{a}_2 \otimes \mathbf{a}_3)| \\ &\leq \left| \mathbf{a} \cdot (\mathbf{b} \times \mathbf{c}) - \tilde{\mathbf{a}} \cdot (\tilde{\mathbf{b}} \times \mathbf{c}) \right| + \left| \mathbf{a} \odot (\mathbf{b} \otimes \mathbf{c}) - \tilde{\mathbf{a}} \cdot (\tilde{\mathbf{b}} \times \mathbf{c}) \right| \\ &\leq \frac{1}{\sigma} \det(\mathbf{A}) \mathcal{O}(\epsilon_{\text{machine}}). \end{aligned}$$

□